Journal of Molecular Structure 1381 (2027) 147364

Contents lists available at ScienceDirect

Journal of Molecular Structure

journal homepage: www.elsevier.com/locate/molstr

Photoluminescent Lanthanide(III) complexes from β-diketonate and terpyridine isomers: structural and energy-transfer insights

Zafar Abbas [a,1], Usha Yadav [a,1], Ray J. Butcher [b], María Joaquina Beltrán-Leiva [c], Julián Santoyo-Flores [c], Dayán Páez-Hernández [c,d], Ashis K. Patra [a,*]

[a] Department of Chemistry, Indian Institute of Technology Kanpur, Kanpur, Uttar Pradesh, 208016, India
[b] Department of Chemistry, Howard University, Washington DC, 20059, USA
[c] Doctorado en Fisicoquímica Molecular, Universidad Andres Bello, República, Santiago, 275, Chile
[d] Center of Applied Nanoscience, Universidad Andres Bello, República, Santiago, 275, Chile

ARTICLE INFO

Keywords:
Molecular structures
Lanthanide luminescence
Energy transfer pathways
Theoretical calculations
Fragmentation scheme

ABSTRACT

A set of structurally isomeric Ln^{III} complexes: [Ln(RnTPY)$(TTA)_3$] (**1–9**), where Ln = Eu^{III} (**1–3**), Sm^{III} (**4–6**), Dy^{III} (**7–9**), Rn = n-pyridyl (n = 2, 3 and 4, refers to the position of N in 4'-pyridyl ring), TPY = 2,2′:6′,2″-terpyridine, and TTA = 1,1,1-trifluoro-3-(2-theonyl)acetone were studied. These ternary dual-sensitized Ln^{III}-complexes were thoroughly characterized in solution using various spectroscopic measurements and their molecular structures were established using X-ray crystallography. They exhibit discrete nine-coordinated {LnN_3O_6} coordination polyhedra showing the tricapped trigonal prismatic (TTP) geometry. We explored the energy transfer pathways from the ligands to metal ion and attempted to evaluate any electronic effects of changing the orientation of the positional isomeric n-pyridyls conjugated to the terpyridine (RnTPY) backbone-derived isostructural Ln^{III}-complexes in energy-transfer using multireference CASSCF/PT2 theory. The theoretical calculations were performed through a fragmentation method, therein all the fragments (TTA, RnTPY, and Ln^{III}) were treated at the same level of theory. The energy gaps ($\Delta E_{3T\rightarrow Ln^*}$) between the ligand-localized triplet state (^3T) and the emitting levels of the Ln^{III} fragments (Ln*) were determined to elucidate the most probable ET-pathways. These theoretical observations and the calculated energy gaps (ΔE) between the ^3T states of the antennae and the emissive excited state of Ln^{III} give an insight into the trends in the sensitization efficiency of the Ln^{III}-fragments. The excited states of Eu^{III} and Sm^{III} are effectively populated, while sensitization was found ineffective in the Dy^{III}-containing systems. The calculations successfully ascribe the in general sensitization mechanism in [Ln(RnTPY)$(TTA)_3$] from the antennae and electronic effects arising from the positions of Ns of n-pyridyls in the RnTPY antenna.

1. Introduction

The luminescent lanthanide materials have potential applications in display devices, optical amplifiers, tuneable lasers, upconversion materials, medical diagnosis, therapy, etc. [1–6]. Ln^{III} materials have uniquely distinct optical parameters, like high colour purity, sharp and bright emissions in the wider optical range, large ligand-induced pseudo-Stokes shifts, and long-lived excited state lifetime (μs-ms) [7]. These advantageous luminescence properties of Ln^{III} arise from the characteristic *f-f* transitions in their inner 4*f* shell, which is shielded by the outer 5 s and 5p shells [8,9].

Lanthanide $4f^n-4f^n$ transitions suffer from poor molar absorptivity ($\varepsilon \leq 1$ $M^{-1}cm^{-1}$) attributed to their spin-forbidden transition by Laporte's selection rule which makes the direct excitation of the Ln^{III} inefficient [10,11]. Thus, indirect sensitization achieved *via* conjugating chromophoric ligand(s) to the Ln^{III}, which effectively harvests and transfers the energy to the excite states of the Ln^{III}* ion, known as antenna effect [12–15]. The selection of a suitable antenna require clear understanding of its electronic structure and energy levels compared to the relevant Ln^{III} energy states [16–18]. Tailoring of excited-state energies by peripheral substituents with coordinating aromatic *N*-donor ligands could be potentially used as antenna to sensitize Ln^{III} luminescence due to their strong absorbance [19,20]. A well-established energy transfer (ET) pathway for the emissive Ln^{III} system is: ligand (^1S)→

* Corresponding author.
E-mail address: akpatra@iitk.ac.in (A.K. Patra).
[1] Equal contribution.

https://doi.org/10.1016/j.molstruc.2026.147364
Received 1 January 2026; Received in revised form 31 July 2026; Accepted 14 August 2026
Available online 15 August 2026
0022-2860/© 2026 Elsevier B.V. All rights are reserved, including those for text and data mining, AI training, and similar technologies.

ligand(^3T)→[Ln^{III}]*→[Ln^{III}]. Moreover, the Ln^{III} complexes should be coordinatively saturated to minimize the non-radiative quenching *via* vibrational energy transfer (VET) to the surrounding O—H, N—H, and C—H oscillators [12,21,22].

Typically, TTA is a suitable β-diketonate ligand for Ln^{III} due to their facile complexation that drives high thermodynamic stability. The β-diketonate containing Ln^{III}-complexes show superior photophysical properties, effective sensitization, higher quantum yields, high colour purity, etc. [23–25]. The [$Ln(TTA)_3(X)_n$] (X= solvent, anions) precursors could be used to coordinate the neutral *N*-donor ligands (TPY, BPY, phen) to serve as secondary antenna or to incorporate rich photochemistry [26–28]. Such additional sensitizers also prevents the nonradiative vibrational quenching deactivation of Ln^{III} luminescence by removing the O−H oscillator of H_2O and allowing the fine-tuning of photoluminescence properties. Thus, Ln^{III} complexes derived from β-diketonate, and heterocyclic N-donor ligands gained increasing attention and established their application in light-emitting diodes (OLED), polymers, and solar cells, crystal glasses, thermometry devices, pH sensors, chiral sensing, antibody labels, and bio-imaging agents [29–32].

It is important to emphasize that the photophysical properties of Sm^{III} and Dy^{III} complexes have received less attention than Eu^{III} ions [33,34]. The extent of luminescence quenching is inversely proportional to the energy gap ($\Delta E_{Ln\text{-}Ln^*}$) between the emissive and ground states of Ln^{III} ions. Thus, Sm^{III} and Dy^{III} complexes suffers inherent disadvantage of lower luminescence intensity because of the smaller $\Delta E_{Ln\text{-}Ln^*}$ of ca. 7400 cm^{-1} for Sm^{III}, 7850 cm^{-1} for Dy^{III} , while for Eu^{III}, $\Delta E_{Ln\text{-}Ln^*}$ =12, 300 cm^{-1}, which is quite large [35,36]. Furthermore, effective deactivation of these Sm^{III} and Dy^{III} excited states also occurred by the high energy oscillators (O–H ~ 3300–3500, N–H ~ 3100–3300, and C–H ~ 2950 cm^{-1}) of the solvents or these oscillators within the coordinated ligands [37–39]. These causes effectively results in quenching of luminescence and lower luminescence quantum yields from these complexes. The luminescent lanthanide materials were widely explored for diverse optical applications; however, the investigation around the involvement of associated electronic states of the antennae, lanthanides energy states, and accurate ET mechanism and pathways are still going on and not yet fully understood [40–43]. Sometime, the proposed electronic energy transfer is only generic with associated misconception due to over-simplification and absence of quantitative theoretical studies. Therefore, it is essential to have a more quantitative molecular-level description of the electronic states and their energy gaps to propose a convincing and accurate ET-mechanisms from the antenna to the Ln^{III}-ions. The output from such theoretical calculations is a valuable aid for designing and fine-tuning the electronic structure of the antenna to obtain bright and functional luminescent lanthanide materials.

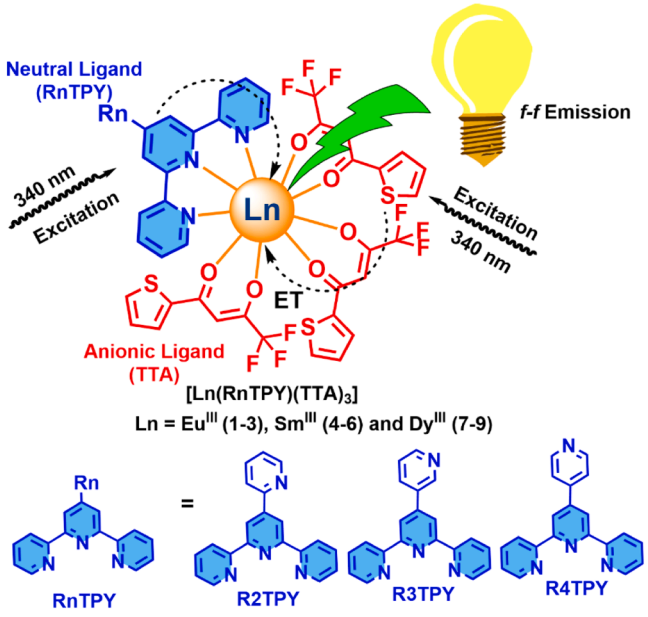
A limited theoretical tools, models and protocols concerning electronic energy transfer in lanthanides are reported in literature. Tanner et al. critically reviewed and addresses the existing misconceptions involved in the ET mechanisms in Ln^{III} ions and offered in-depth overview of alternative ET theories [40]. Malta et al. introduces detailed theoretical approaches for ET mechanism from ligands to the Ln^{III} ions and determined their quantum efficiency [41,42]. M. J. Beltrán Leiva et al. performed theoretical studies of luminescent lanthanides complexes derived from neutral NˆN-donor antenna and elucidated their ET-mechanisms extensively [44,45]. Recently, our group strategically designed a series of luminescent Eu^{III} and Tb^{III} complexes and evaluated their ET pathways using advanced theoretical models [46].

Herein, we attempted to evaluate the plausible energy-transfer modes and effects on the associated electronic states due to substitutionally varying orientations of the n-pyridyls at 4′-position of the TPY antennae (RnTPY) in the series of lanthanide complexes as shown in **Scheme 1**. The energy levels of all the fragments (Ln^{III}, RnTPY, TTA) were determined using CASSCF/PT2-based calculations and probable ET-pathways from the antenna to the excited emissive states of Ln^{III} ions were proposed. For a systematic study, we have synthesized a series of isostructural nine-coordinated [Ln(RnTPY)$(TTA)_3$] (Ln = Eu^{III} (**1–3**), Sm^{III} (**4–6**), Dy^{III} (**7–9**)) complexes with varied RnTPY ligands. The complexes were derived from three unsymmetrical β-diketonate (TTA) antennae and N2/N3/N4-positioned 4′-pyridyl terpyridine antenna (RnTPY, Scheme 1) judiciously substituted at the *p*-position. The TTA ligands are expected to provide thermodynamic stability, and act as a sensitizer for Ln^{III} ions. The substituted terpyridines envisioned to have subtle effects on the singlet and triplet state of TPY ligands, consequently affecting the electronic property of the Ln^{III}-complexes. A detailed structural characterization of the complexes (**1–7**) was performed using single crystal X-ray crystallography and photophysical studies in solution. In case of [Ln(RnTPY)$(TTA)_3$] (**8** and **9**) complexes (Ln = Dy^{III}, Rn = R3, R4) geometries were optimized using the [Dy(R2TPY)$(TTA)_3$] (**7**) coordinates as reference. Thereafter, advanced multiconfigurational *ab initio* theoretical methodology combined with scalar relativistic time-dependent DFT were chosen to calculate the energies of electronic states in the complexes and the ligands involved in energy transfer and emission from Ln^{III} ions. All the ligands and Ln^{III} ions were treated at the same level of theory using *ab initio* wavefunctions to achieve acceptable solutions to determine the energy transfer pathways and effect of terpyridine substitution on the electronic states and photophysical properties of the complexes [26,44,45].

2. Result and discussion

2.1. Synthesis and general aspects

A series of heteroleptic complexes of general formulation: [Ln(RnTPY)$(TTA)_3$] (**1–9**) containing positional isomeric 4′-pyridyl-terpyridine ligands (RnTPY) and TTA β-diketonate ligands were synthesized by mixing [$Ln(TTA)_3{\cdot}3H_2O$] precursor complex (1.0 eq.) and RnTPY derivatives (1.2 eq.) in THF. The desired products were precipitated out by adding an excess of hexane into the concentrated THF solution of complexes in high yield (~ 70%). These complexes were characterized by NMR, FT-IR, ESI-MS studies and molecular structures were determined by X-ray crystallography. The isostructural crystalline complexes stable in ambient conditions and show good solubility in



Scheme 1. Molecular design principle for [Ln(RnTPY)$(TTA)_3$] (**1–9**) showing the photosensitization and energy-transfer pathways from the antennae (TTA, RnTPY) to the Ln^{III}-center for *f-f* emission. The structures of RnTPY ligands are shown at the bottom. RnTPY = n-pyridyl 2,2′:6′,2″-terpyridine (n = 2, 3 and 4), and TTA = 1,1,1-trifluoro-3-(2-theonyl)acetone.

polar solvents, i.e., chloroform, THF, acetone, acetonitrile, DMF, DMSO, etc. The ESI-MS analysis of all the complexes **1–9** showed the cationic molecular ion peaks (*m/z*) assigned to $[M\text{-}TTA]^+$ of the respective [Ln(RnTPY)$(TTA)_3$] complexes in DMF. The matching and characteristic isotopic distribution pattern to the respective Eu^{III}, Sm^{III} and Dy^{III} ions, signifies the exclusive formation of isostructural mononuclear complexes and their structural integrity in solution **(Fig. S1-S9, ESI)**. The FT-IR spectra of complexes **1–9** were found nearly identical in the fingerprint region, suggesting their similar chemical bonding and isostructural nature in the solid-state **(Fig. S10, ESI)**. A strong stretching frequency at ~1612 cm^{-1} attributed to the $\nu_{C=O}$ stretching vibrations of the coordinated β-diketonate ligand (TTA). The shift of $\nu_{C=O}$ from ~1676 cm^{-1} in the free HTTA to 1600 cm^{-1} in the complexes **1–9** provides strong evidence of ionic bonding of anionic O, O-donor TTA^- to the Ln^{III} ion. The FT-IR peaks at ~1583, 1584 and, 1582 cm^{-1},respectively, for the R2TPY, R3TPY, and R4TPY ligands were attributed to C═N stretching frequencies of the RnTPY ligands. The Ln–O(TTA) and Ln–N(RnTPY) stretching frequencies appears at 490 cm^{-1} to 520 cm^{-1} respectively [28,45,47]. The FT-IR spectra and their close resemblance provide direct evidence for Ln^{III} ions coordination to TTA and RnTPY ligands in this series of analogous [Ln(RnTPY)$(TTA)_3$] complexes. The

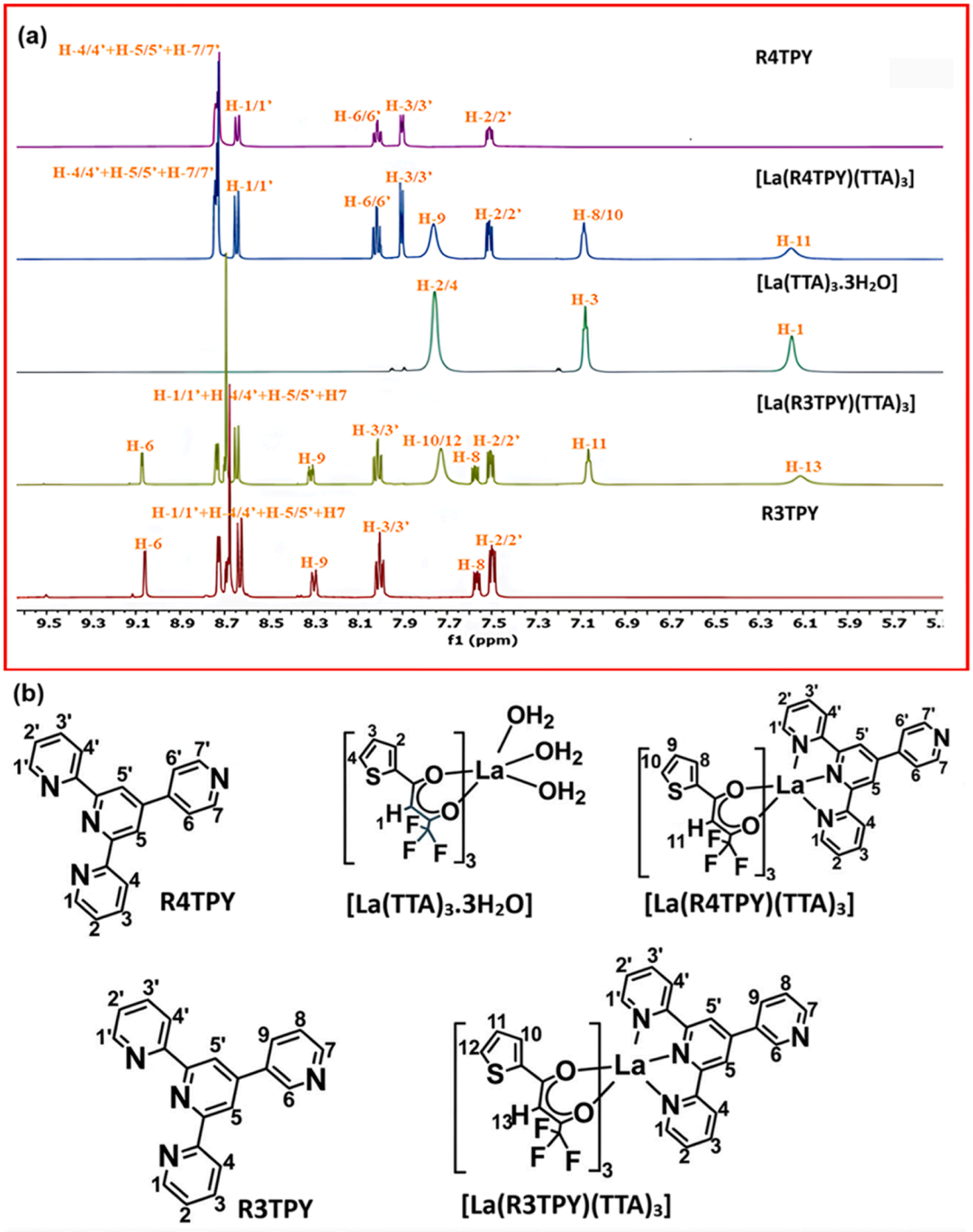


Fig. 1. (a) ^{1}HNMR stacked spectra of the ligand R3TPY, [La(R3TPY)$(TTA)_3$] complex, precursor complex [La$(TTA)_3{\cdot}2H_2O$], [La(R4TPY)$(TTA)_3$] complex and ligand R4TPY, respectively in DMSO-d_6, 500 MHz **(b)** Chemical structure of the molecules with proposed assigned protons as shown in the stacked spectra.

NMR spectroscopy is an important tool to characterize and identify the molecular structures and stability to establish the complex formation in solution. Most paramagnetic Ln^{III}-complexes results in significant spectral broadening, large chemical shifts and complexity in their ^{1}HNMR signals [48]. However, the structurally analogous diamagnetic Lanthanum (La^{III}) complexes could provide a good alternative and avoid such limitations. Therefore, to facilitate ^{1}HNMR characterization, we synthesized diamagnetic [La(R3TPY/R4TPY)(TTA)$_3$] complexes as structural analogues of the corresponding paramagnetic [Ln(RnTPY)(TTA)$_3$] complexes. The ^{1}H-spectra of [La(R3/4TPY)(TTA)$_3$] showed a set of resonance peaks characteristic of La^{III}-bound R3/4TPY and TTA ligands, confirming their solution stability. The labelling and proposed assignment of corresponding chemical environments for the ^{1}HNMR signals were shown in Fig. 1. Overall, the number of protons, chemical shifts, and relative intensities observed in the ^{1}HNMR spectra are consistent with the proposed stoichiometry, formulation, and solution stability of the complexes.

2.2. Structural characterization

The molecular structures of [Ln(RnTPY)(TTA)$_3$] (**1–7**) complexes were elucidated by single-crystal X-ray crystallography (Fig. 2, **Fig. S11**). Diffraction quality crystals were grown in a combination of solvents and varied conditions. All the complexes showed similar coordination environment around respective Ln^{III} ions and only differ by the nature of n-pyridyl substituents (Rn) in RnTPY ligands. The Ln^{III} centre coordinated with three anionic β-diketonate (OˆO)-donor TTA and one neutral (NˆNˆN)-donor RnTPY ligand, forming nine-coordinated {LnN$_3$O$_6$}-coordinated tricapped trigonal prismatic (TTP) geometry. The selected crystallographic parameters are given in **Tables S1-S3** and selected bond lengths and angles were given in **Tables S4 and S5** in ESI. Three mono-anionic OˆO-donor TTA ligands neutralizes the tri-positive Ln^{III} ions *via* ionic bonding. The Ln(Eu^{III}/Sm^{III}/Dy^{III})–N(RnTPY) bond lengths lies in the range of 2.533–2.624 Å, whereas the bond lengths of Ln(Eu^{III}/Sm^{III}/Dy^{III})–O(TTA^-) anionic TTA ligands ranges in 2.326–2.451 Å. Obviously, the anionic TTA^- (OˆO) shows stronger ionic binding to Ln^{III} cations compared to the neutral RnTPY ligands. The ∠N(1)–Ln–N(3) bite angles for the neutral ligand were approximately 114.04°−126.80°, while ∠O–Ln–O for the TTA ligands was in the range of 68.17–149.69° Further crystal packing analysis of these complexes reveals π-π stacking between the aromatic rings that contributes to the stability of the supramolecular architecture (**Fig. S12-S14,** ESI). [Ln(R2TPY)(TTA)$_3$] complexes show weak (4.101–4.658 Å) π-π stacking interactions between the adjacent molecules through pyridine rings of the R2TPY ligands. Stronger stacking interactions (3.653 and 3.664 Å) were observed for [Eu(R4TPY)(TTA)$_3$] and [Sm(R4TPY)(TTA)$_3$] through the terminal pyridine rings. In complexes [Eu(R3TPY)(TTA)$_3$] and [Sm(R3TPY)(TTA)$_3$], stronger π-π interactions (3.585 and 3.649 Å) were observed between the pyridine rings of R3TPY and thiophene ring of the TTA ligands between the adjacent molecules. Overall, these interactions contribute to the crystal packing stability. We failed in our attempts to get diffraction quality crystals of the [Dy(R3TPY)(TTA)$_3$] (**8**) and [Dy(R4TPY)(TTA)$_3$] (**9**). However, molecular structures of complexes **8** and **9** were confirmed by FT-IR spectroscopy and mass spectrometry, as described in the previous section. Both complexes exhibited characteristic absorption bands and mass fragmentation patterns comparable to those observed for complexes **1**–**7**, indicating that complexes **1**–**9** are isostructural. Notably, all the structures contain several residues which are disordered, especially at their thiophene rings, one CF_3 group of the TTA ligand and terminal pyridine rings of the RnTPY ligands and damp command was applied for the refinement to converge. Such residual disorders are well-documented in the literature [46,49–51]. The ORTEP view of complexes **1–7** were shown in Fig. 2, and **Fig. S11** and unit cell packing diagrams were shown in **Fig. S15-S18** in **ESI**.

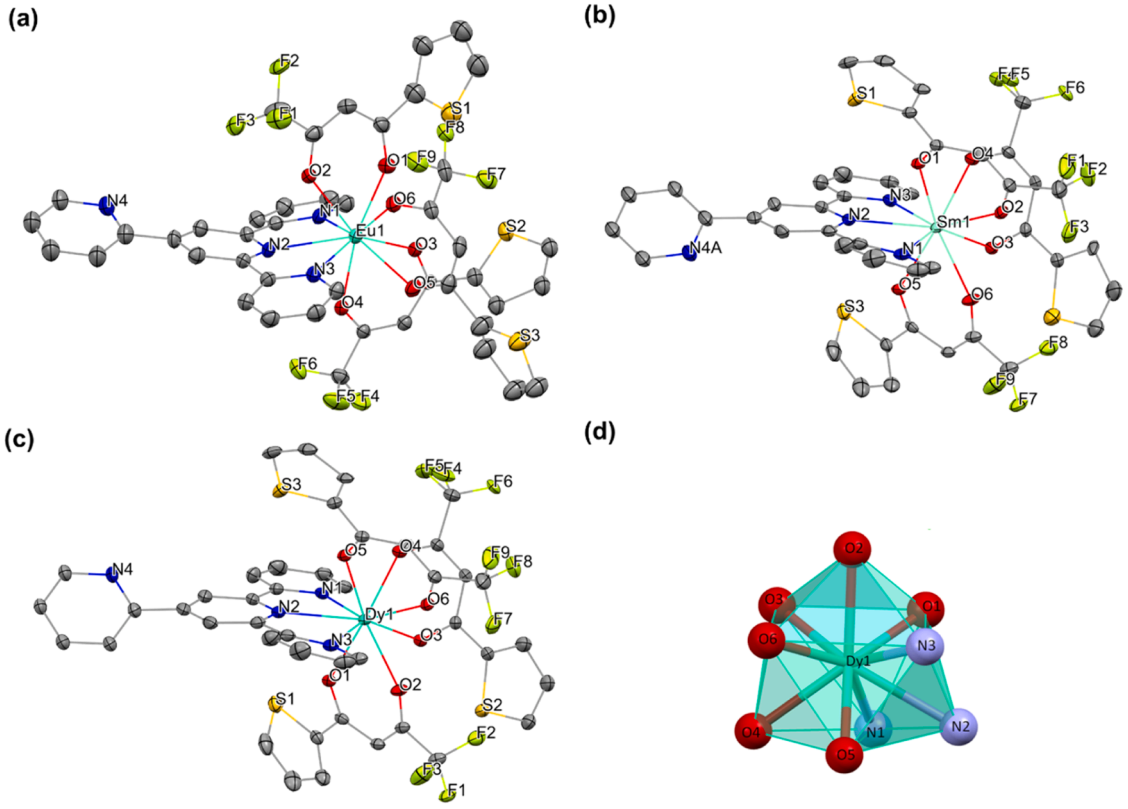


Fig. 2. The ORTEP views of complexes **(a)** [Eu(R2TPY)(TTA)$_3$] (**1**), **(b)** [Sm(R2TPY)(TTA)$_3$] (**4**), and **(c)** [Dy(R2TPY)(TTA)$_3$] (**7**) with thermal ellipsoids drawn at 30% probability level with atom labelling schemes for the metal and the ligands. **(d)** Coordination polyhedra of the lanthanide core for complex **7** showing {DyO$_6$N$_3$} tricapped trigonal prismatic (TTP) geometry.

2.3. Photophysical properties

2.3.1. Electronic absorption

The electronic energy states of the conjugated antenna drive the unique optical properties of the synthesized [Ln(RnTPY)(TTA)$_3$] complexes *via* indirect energy-transfer pathways. The electronic absorption and photoluminescence spectral studies of the ligands (RnTPY and TTA) and their [Ln(RnTPY)(TTA)$_3$] complexes measured in acetonitrile (MeCN) were shown in Fig. 3**(a)/3(b)** and **Fig. S19-S25(ESI)**. The absorption bands for the derivatives of RnTPY appears at ~270 nm and a shoulder at ~327 nm attributed to the ligand-centered π–π^* and n–π^* transitions of the aromatic moieties of RnTPY. However, the absorption maxima (λ_{max}) of the free HTTA ligand centred at 342 nm assigned to its π–π^* transition as shown in Fig. 3**(a)**. The absorption spectra of all the Ln^{III}-containing complexes **(1–9)** show two ligand-centred electronic transition bands at 280 nm and at 336 nm, desirable for the indirect sensitization of the representative Ln^{III}-complexes shown in Fig. 3**(b) and Fig. S19 and S20 (ESI)**.

2.3.2. Photoluminescence

[Eu(RnTPY)(TTA)$_3$] (1–3): To understand the energy-transfer (ET) mechanisms between the ligands (TTA, RnTPY) to the Eu^{III} ion in their Eu^{III}-containing systems, we recorded the absorption spectra of the respective ligands and the photoluminescence -excitation spectra (PLE) of [Eu(RnTPY)(TTA)$_3$] complexes **(Fig. S21, ESI)**. These spectral data advocates that TTA ligands are well-overlapped with the excitation spectra of Eu^{III}-complexes compared to RnTPY ligands suggesting TTA is an effective sensitizer for emissive state of Eu^{III} ion, supported by previous literature precedence [26,29,51]. Subsequently, their photoluminescence (PL) spectra were recorded at the lowest energy excitation bands (λ_{ex} = 340 nm) showing sharp intense luminescence peaks in the visible region attributed to $^5D_0$–$^7F_1$ (592 nm, MD), $^5D_0$–$^7F_2$ (615 nm, Forced ED), $^5D_0$ –$^7F_3$ (653 nm, MD), and $^5D_0$–$^7F_4$ (704 nm, Forced ED) transitions characteristic of the Eu^{III} ions as shown in Fig. 3**(c)**.The most intense hypersensitive $^5D_0$–$^7F_2$ transition at 615 nm is primarily responsible for the bright red luminescence of the Eu^{III}-containing systems. Notably, a closer observation of the PLE and PL spectra of [Eu(RnTPY)(TTA)$_3$] (**1, 2**) derived from R2TPY /R3TPY ligands showed comparatively higher intensity than that of the analogous Eu^{III} complex from R4TPY ligand system suggesting that the former two ligands exhibit relatively better sensitization than R4TPY ligand. The intensity ratio (R_{Eu}) of I_{7F2}/I_{7F1} is a measure of asymmetry around the Eu^{III} ion and this ratio is comparable for **1–3** (I_{7F2}/I_{7F1} = 23.52 (**1**) ≈ 23.20 (**2**) ≈ 22.80 (**3**) in MeCN). The close I_{7F2}/I_{7F1} ratio is indicative of similar coordination atmosphere around the Eu^{III} ions in [Eu(RnTPY)(TTA)$_3$] (**1–3**). Steady-state emission spectra of the Eu^{III}-containing systems exhibit weak ligand-based emission at ~371 nm characteristic of the RnTPY ligand **(Fig. S25)**, whereas intense typical Eu^{III}-centred emission was observed **(Fig. S23),** suggesting an efficient energy transfer from antenna molecules to emissive excited states of the metal ion. To further confirm the structural integrity of the complexes and absence of any coordinated solvent or water molecule with the Ln^{III} in solution, we measured the luminescence lifetimes (τ) of **1–3** in H_2O and D_2O and calculate the hydration numbers (q) using a modified Horrocks equation [52]. The hydration number, $q < 1$ suggests absence of any inner-sphere H_2O molecules in the tested coordinatively-saturated complexes with {LnN$_3$O$_6$} polyhedra and retain maintain structural integrity in solution as shown in their solid-state structures shown in Fig. 4**(a, b) and Fig. S26 (ESI)**.

[Sm(RnTPY)(TTA)$_3$] (4–6): In the case of Sm^{III}-complexes, the PL spectra upon λ_{ex} = 340 nm showing sharp intense peaks in the visible region at 564, 600, 646 and 706 nm respectively corresponds to $^4G_{5/2}$–$^6H_{5/2}$, (564 nm, MD), $^4G_{5/2}$–$^6H_{7/2}$ (600 nm, ED+MD), $^4G_{5/2}$–$^6H_{9/2}$ (647 nm, ED) and $^4G_{5/2}$–$^6H_{11/2}$ (706 nm, forbidden) as shown in Fig. 3 **(d)**. The intensity of the forbidden $^4G_{5/2}$–$^6H_{11/2}$ (ΔJ = 3) transition is very less. The intensity ratio (R_{Sm}) of ($I_{6H9/2}/I_{6H5/2}$) measures the asymmetry around the Sm^{III} ion. The R_{Sm} value for these complexes were: 6.49 (**5**) ≈ 6.40 (**4**) ≈ 6.16 (**6**) in MeCN. The closer R_{Sm} values

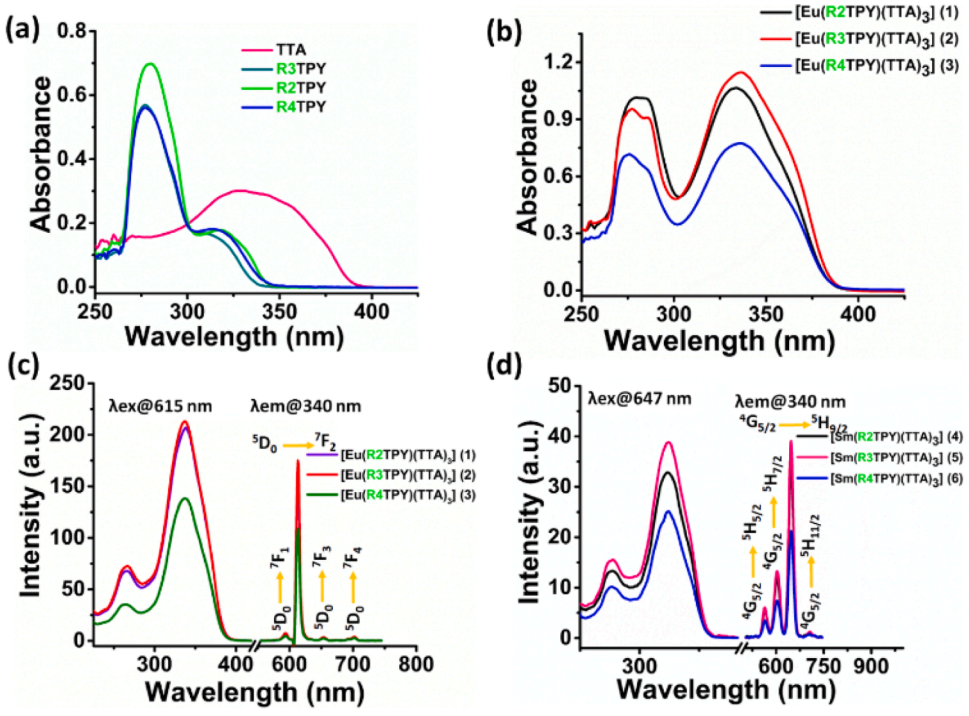


Fig. 3. Electronic absorption spectra of **(a)** RnTPY and TTA ligands (20 μM) and **(b)** [Eu(RnTPY)(TTA)$_3$] (**1–3**) in MeCN (20 μM) at 298 K. **(c)** Excitation and emission spectra of Eu^{III}-complexes (**1–3**) showing characteristic $^5D_0$–^7F_J transitions corresponding to Eu^{III}-ions in MeCN (2 μM); λ_{ex} = 340 nm, Ex./Em. slit width = 2.5/2.5 nm. **(d)** Excitation and emission spectra of [Sm(RnTPY)(TTA)$_3$](**4–6**) showing characteristic $^4G_{5/2}$–^6H_J transitions corresponding to Sm^{III} -ions in MeCN (2 μM) with strong $^4G_{5/2}$–$^6H_{5/2}$ transition. λ_{ex} = 340 nm, Ex./Em. slit width = 2.5/2.5 nm.

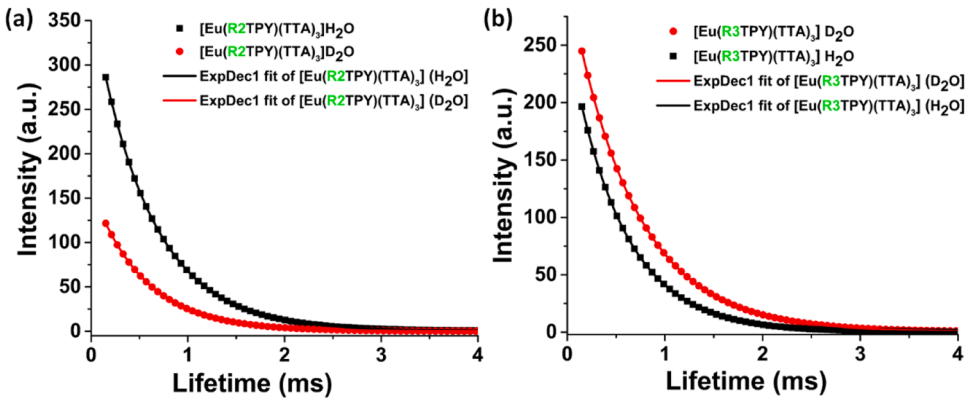


Fig. 4. Luminescence decay profile for $^5D_0$–$^7F_2$ transition and lifetime measurements at 615 nm for **(a)** [Eu(R2TPY)(TTA)$_3$] (**2**) and **(b)** [Eu(R3TPY)(TTA)$_3$] (**3**) in H_2O and D_2O (14 μM) at 298 K. λ_{ex} = 340 nm, delay time and gate time = 0.1 ms, total decay time = 3.0 ms, Ex. and Em. slit width = 5 nm.

signify a near identical environment around the Sm^{III} ion in **4–6**. The significant overlap of the absorbance spectra of TTA ligand and the excitation spectra **1–6** complexes also suggests that predominately TTA antenna populates the excited emissive levels of Eu^{III} and Sm^{III}-ions **(Fig. S22, ESI)**. Notably, the R2TPY and R3TPY derived [Sm(RnTPY)(TTA)$_3$] (**4, 5**) complexes showed relatively higher intensities than [Sm(R_4TPY)(TTA)$_3$](**6**) as observed for the isostructural Eu^{III}-complexes. This observation suggests that R2TPY/R3TPY ligands are apparently better sensitizer than the R4TPY under identical experimental conditions. Steady-state emission spectra of the complexes **4–6** showed characteristic Sm^{III} ion centred emission along with ligand-centred emission bands at ~371 nm for RnTPY ligands **(Fig. S24)**. A weaker luminescence was observed for the Sm complexes (**4–6**) compared to the Eu complexes (**1–3**), owing to less efficient energy transfer caused by competing non-radiative processes, as previously reported [53–55].

[Dy(RnTPY)(TTA)$_3$] (7–9): Similar photophysical studies were performed for complexes **7–9**. However, under the same experimental conditions used for complexes **1–6**, no characteristic emission bands corresponding to Dy^{III} were observed in solution. At first glance, this behaviour might suggest that the employed ligands are not able to efficiently sensitize the Dy^{III} emissive level. However, considering the multicomponent antenna system present in these complexes, the absence of emission is more likely attributed to the competing deactivation pathways, rather than a simple mismatch of energy levels. In particular, the presence of the TTA ligand, which possesses a relatively low-lying triplet state, may introduce additional non-radiative relaxation channels that can quench the excited state of Dy^{III}. The measured experimental photophysical parameters of the complexes **1–9** were summarized in Table 1. To clarify the origin of this behaviour, identifying the dominant energy-transfer pathways, and role of TPY substitution, if any, on the optical properties of complexes **1–9,** theoretical calculations were performed to determine the relative energies of the ligand and lanthanide excited states.

Theoretical Calculations: The theoretical calculations were performed to evaluate the electronic states of the antenna ligands, possible substituent effects, and to have a detailed insight into the possible energy-transfer (ET) pathways from the ligands to Ln^{III} and understand the photophysical properties of the designed Ln^{III} complexes. For the sake of simplicity, the discussion about the electronic structure is presented here separately for both the entire Ln(III) complexes and ligand fragments.

2.3.3. Spectroscopic properties of the ligands

The theoretical approach is important to calculate the electronic energy levels of the ligands, especially the lowest triplet states of the antenna, involved in energy-transfer to the Ln^{III}-ions. The energy-transfer from the lowest triplet state (T_1) of antenna ligand to the excited state of lanthanide ion is commonly accepted sensitization pathway [26,56–58]. The quality of the fragmentation approach employed herein is directly related to the accuracy in the determination of electronic states of the ligands. According to the CAS (8, 8) SCF/PT2-based calculations, the substituted terpyridine (RnTPY) ligands have T_1 states located ~ 30,000 cm^{-1} regardless of the substituent **(see Table S6-S8, ESI)**. It suggests that the energy of the T_1 states is insensitive to the position of N-atom in the outer pyridine ring. In the case of TTA ligand, the T_1 state was determined uniformly at ~21, 000 cm^{-1},which is in correct agreement with previous *ab–initio* calculations performed on this ligand [4]. Theoretically calculated data suggest that there are no significant energy differences in the T_1-energy levels were observed among the RnTPY derivatives (Table 2, **S7** and **S8, ESI**). This observation suggests that the isomeric position of the

Table 1
UV–Vis absorption, lifetimes (τ), and hydration number (q) of complexes **1–9** .

Ln(III)-Complexes	UV–Vis[a] (ε [$M^{-1}cm^{-1}$])	τ_{DMF} (ms)[b]	τ_{H2O} (ms)[c]	τ_{D2O} (ms)[d]	q[e]
Eu (**1**)	336 nm (52,842), 280 nm (50,742)	0.617	0.532	0.588	0.09
Eu (**2**)	336 nm (57,370), 280 nm (46,797)	0.572	0.528	0.562	0.17
Eu (**3**)	336 nm (50,370), 280 nm (46,797)	0.612	0.529	0.535	0.31
Sm (**4**)	336 nm (45,220), 280 nm (37,844)	0.106	-	-	-
Sm (**5**)	336 nm (40,624), 280 nm (37,162)	0.100	-	-	-
Sm (**6**)	336 nm (38,954), 280 nm (34,365)	0.109	-	-	-
Dy (**7**)	336 nm (46,278), 280 nm (54,452)	-	-	-	-
Dy (**8**)	336 nm (41,600), 280 nm (48,880)	-	-	-	-
Dy (**9**)	336 nm (41,105), 280 nm (53,294)	-	-	-	-

[a]Electronic absorption in acetonitrile, ε = Molar absorptivity. [bcd]Luminescence lifetime in H_2O and D_2O ($\tau \pm 10$ %). [e]Determination of inner-sphere hydration number using modified Horrocks' equation ($q \pm$ 10 %).

Table 2
First two excited singlet (S) and triplet states (T) of the ligands taken from the [Eu(RnTPY)(TTA)$_3$]. All the values are given in cm^{-1}.

State	R2TPY	[TTA]$^-$	R3TPY	[TTA]$^-$	R4TPY	[TTA]$^-$
S_1	34,777	29,524	34,634	25,128	29,418	26,203
S_2	35,545	29,907	35,941	25,538	34,555	28,393
T_1	30,207	21,801	30,377	20,286	27,559	22,268
T_2	31,391	25,794	31,319	23,745	29,835	28,393

pyridyl-*N* as peripheral substituent do not perturb the energy states of the RnTPY ligand significantly. It is also evident from the energy level diagram that TTA is not a suitable sensitizer for Dy^{III} complexes because it possesses higher energy emissive excited states than the triplet level of the feeding state (Fig. 5c and **Fig. S27** in ESI). Despite the availability of high-energy RnTPY triplet state and feasibility of energy transfer from it, there is a possibility of competing back-energy transfer (BET) from the $^6F_{9/2}$ state of Dy^{III} ion to the low lying T_1 state of TTA, suppressing the characteristic Dy^{III} emission from complexes (**7–9**) [59–61].

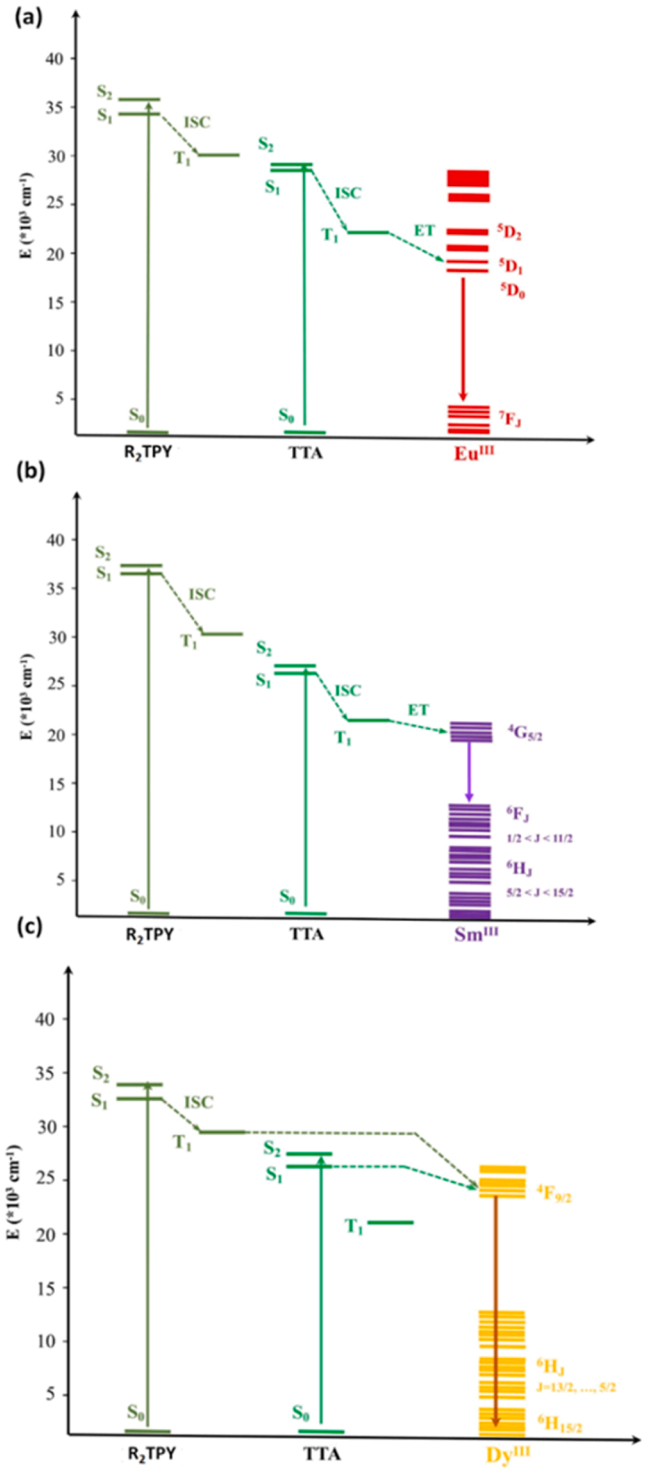


Fig. 5. Jablonski diagram for the most probable energy-transfer pathways in the **(a)** [Eu(R2TPY)(TTA)$_3$] (**1**), **(b)** [Sm(R2TPY)(TTA)$_3$] (**4**) and **(c)** [Dy(R2TPY)(TTA)$_3$] **(7)** complexes. All the energy states were calculated at the CAS/PT2 level of theory, using an active space of CAS (8, 8) for the ligand and CAS (6, 7) for the lanthanide fragments. Different colours reflect different fragments in the overall ET processes. Definitions: ISC, intersystem crossing, ET, energy transfer; VR, vibrational relaxation.

2.3.4. *Electronic states of the Ln^{III}-fragments*

The predicted electronic ground multiplets were characterized by the total angular momentum quantum number (J), correspond to their respective Russell-Saunders notation as $^6H_{5/2}$, $^7F_0$, and $^6H_{15/2}$ for Sm^{III}, Eu^{III}, and Dy^{III}, respectively. All these terms were correctly reproduced by the SO–PT2 calculations employing the minimal active space in agreement with the experimental data and previous reports using the similar established methodology [45,46,62,63]. Fig. 5 shows the energy levels for the ligand as well as Ln^{III} ion fragments according to scale.

The 4*f*-4*f* transitions are electric dipole (ED) forbidden; however, they are commonly observed, and several theories were proposed in literature for their origin. Presently, the most accepted development comes from the Judd–Ofelt theory, which set new selection rules for the "forced" ED transitions considering symmetry and spin-orbit coupling to explain the phenomenon [64]. According to this theory, if some of the 5*d* characters could be introduced into the 4*f* states, the 4*f* –4*f* transitions would be "partially allowed or relaxed". The same could be attributed to a mixture of multiplicities, for example, observing some quintuplet characters in septuplet wavefunctions in the case of Eu^{III} ion. In this context, and to determine the effects originating from the different substitutions of the 4′-position of terpyridine ligand (RnTPY), the composition of the wavefunction was analysed. Neither the mix of 4*f* and 5*d* states, nor the states with contributions from higher multiplicities were found in any of the systems. It was expected because of the core-like character of the 4*f* orbitals. As observed in the previous works [45,46,62], modifications of the local symmetry around the Ln^{III} ion can produce some degree of mixture of states. However, the modification in the substituent (n-pyridyl) are probably too far from the Ln^{III}-center to have any significant effects on the electronic energy levels of Ln^{III}-fragments.

2.3.5. *Energy transfer pathways*

The determination of the most probable energy transfer (ET) pathways was proposed based on phenomenological rules popularly known as "Latva rules" [65]. Firstly, to get an efficient intersystem crossing (ISC) process, the energy gap between the first excited singlet (S_1) and T_1 ($\Delta E_{S1\text{-}T1}$) states of the antenna ligand should be ~5000 cm^{-1}. Additionally, for an effective ET towards the Ln^{III} center, the T_1 state of antenna should be higher than the resonant emissive levels of the Ln^{III} ion (Ln*). An optimum energy difference ($\Delta E_{T1\text{-}Ln^*}$) has been established as ~2500–3500 cm^{-1}. Thus, employing these optimal energy gaps, the most probable sensitization mechanisms were proposed for these systems.

To facilitate the visualization of these ET pathways, a Jablonski type diagram was elaborated for representative [Ln(R2TPY)(TTA)$_3$] (**1, 4, 7**) **(Fig. 5 and Fig. S27** in ESI). Despite these diagrams explaining in detail the sensitization mechanism, some important points must be highlighted. Firstly, the terpyridine derivatives (RnTPY) do not seem to be effective antennas for Eu^{III}- and Sm^{III}-containing systems. Their T_1 state is ~30,000 cm^{-1}, which implies $\Delta E_{T1\text{-}Ln^*}$ of ~10,000 cm^{-1} in all these cases (Table 2 and Table S6-S8, ESI). Due to this large energy gap, non–radiative pathways become more probable, and the ET process becomes less efficient. Secondly, the TTA ligands have T_1 states ~ 22,000 cm^{-1}, yielding more appropriate ΔE to sensitize Eu^{III} and Sm^{III} complexes. The calculated $\Delta E_{T1\text{-}Ln^*}$ is ~4000 cm^{-1} for Eu^{III} systems and ~1800 cm^{-1} for Sm^{III} systems. Eu^{III}-containing systems seem to be the ideal candidates to be sensitized by the TTA and working cooperatively. Finally, based on the electronic states of RnTPY and TTA antenna ligands, the general sensitization mechanism proposed herein contemplates a dual ET process for Eu^{III} and Sm^{III} complexes: first going cooperatively from RTPY to the TTA ligands and then going from the

TTA to the lanthanide center [$S_{1(RnTPY)} \rightarrow T_{1(RnTPY)} \rightarrow T_{1(TTA)} \rightarrow Ln^*$]. In the Dy^{III}-containing systems, the situation differs from that observed for Eu^{III} and Sm^{III} complexes. The triplet energy of the RnTPY ligands (~30,000 cm^{-1}) yields an energy gap of approximately 5000 cm^{-1} relative to the Dy^{III} emissive level ($^4F_{9/2}$) (**Table S8**, ESI). According to the Latva criterion, this energy difference could in principle allow direct sensitization of Dy^{III} from the RnTPY triplet state. However, the presence of the TTA ligand, which possesses a lower-lying triplet state (~21,000–22,000 cm^{-1}), introduces an additional relaxation pathway. In our dual-antenna complexes, after population of the Dy^{III} excited state by RnTPY, thermally assisted back-energy transfer (BET) from the Dy^{III} level to the TTA triplet state becomes energetically feasible [66]. This process efficiently depopulates the Dy^{III} emissive state and results in non-radiative relaxation through the ligand manifold. Consequently, despite the apparently favourable RnTPY→Dy^{III} energy gap, the Dy^{III} complexes (**7**–**9**) remain non-luminescent experimentally. To optimize the luminescence of Dy^{III} complexes, designing require ligands with a higher-energy triplet state (≥ 23,000 cm^{-1}), such as rigid, electron-deficient, or fluorinated diketonate ensuring the level lies comfortably above the $^4F_{9/2}$ (~20,800 cm^{-1}) level to prevent thermal back energy transfer (BET) [67]. Alternatively, employing mono-antenna architecture, or a multidentate ligand system with a smaller conjugation, having relatively high energy ^3T states (≥ 23,000 cm^{-1}), thereby facilitating the ^3T-Ln* energy transfer, increasing sensitization efficiency and maximizing the metal-centered luminescence [68,69].

A generalized scheme and sensitization pathways for complex **1**–**9** have been shown in Scheme 2. Possibility of several other energy transfer, radiative and non-radiative transition in these complexes cannot completely ruled out. Despite the proposed pathways may look intricate, dual ET transfer processes have been reported before [15].

3. Conclusion

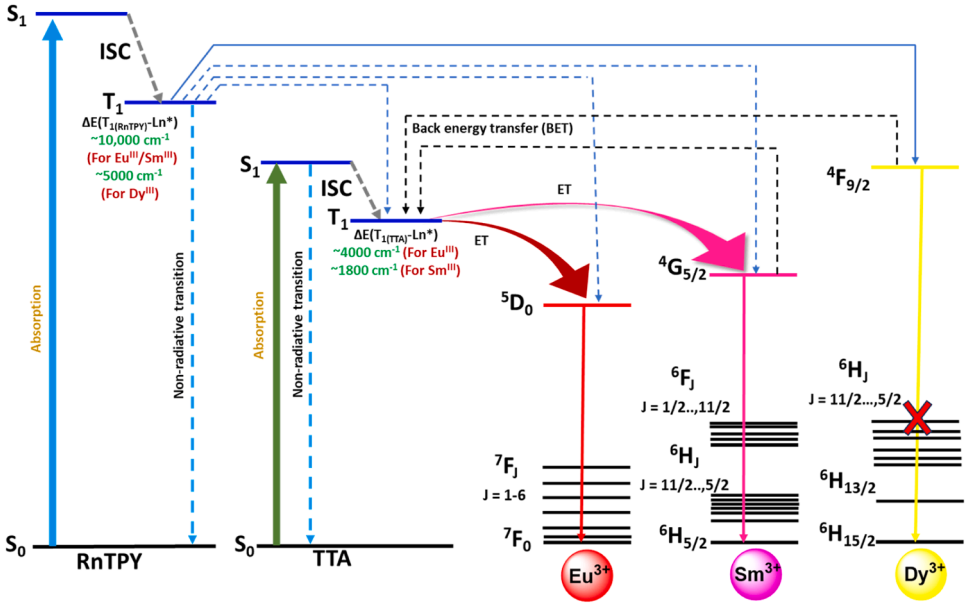
A series of nine heteroleptic Ln^{III}-complexes with the general formula [Ln(RnTPY)$(TTA)_3$] (**1**–**9**) have been synthesized and structurally characterized. They showed discrete nine-coordinated {LnN_3O_6} coordination polyhedra showing the tricapped trigonal prismatic geometry.

We established the solution speciation and the photophysical properties of the complexes. Experimental results suggest better sensitization of Eu^{III} systems over Sm^{III}- complexes by the employed ligands, while Dy^{III}-containing systems remain non-luminescent. Experimentally, we are unable to observe any significant effects of peripheral n-pyridyls of RnTPY ligands in the photophysical properties the designed complexes **1**–**9**. The energy levels of all the fragments (Ln^{III}, RnTPY, TTA) involved in the complex formation (**1**–**9**) were determined on the same level of theory using CASSCF/PT2-based calculations and probable ET-pathways from the ligands to the excited emissive states of Ln^{III} ions were proposed. These theoretical observations and the calculated energy gaps (ΔE) between the ^3T states of the antennae and the emissive excited state of Ln^{III} explain the trends in the sensitization efficiency of the Ln^{III}-fragments. The excited states of Eu^{III} and Sm^{III} systems were effectively populated and displayed characteristic emission. In contrast, the Dy^{III} complexes (**7**–**9**) remain non-luminescent despite the apparently favourable energy gap between the RnTPY triplet state and the Dy^{III} emissive level. Theoretical calculations reveal that the presence of the lower-lying triplet state of the TTA ligand enables thermally assisted back-energy transfer from Dy^{III} in dual-antenna system, which efficiently quenches the Dy^{III} excited state and suppresses the observable emission. The calculations, though successfully ascribe the sensitization mechanism in [Ln(RnTPY)$(TTA)_3$], however remain ineffective in deciphering any major electronic effects arising from the positional orientations of N in peripheral n-pyridyl in the RnTPY antenna for the studied complexes. The results reinforce the idea of changes in the local symmetry around the Ln^{III} ion should have profound effects on their electronic structure, while minor modifications in the distant outer coordination sphere probably will not have major influence on their optical properties.

4. Experimental section

4.1. Materials and methods

Employed reagents and chemicals for the synthesis of ligands and complexes were purchased from chemical suppliers and were used without purification. The organic solvents used for the synthesis and project-related studies were either HPLC grade or purified by standard methods. Precursor complexes [Ln$(TTA)_3 \cdot 2H_2O$] where Ln = Eu^{III}, Sm^{III} and, Dy^{III} were synthesized by literature procedures. ^{1}HNMR studies of analogous terpyridine derivatives (RnTPY) and their complexes were



Scheme 2. The schematic diagram illustrates the probable and effective energy transfer pathways from the ligands (RnTPY and TTA) to the corresponding electronic states of Eu^{III}, Sm^{III}, and Dy^{III} ion (ISC, intersystem crossing; ET, energy transfer; BET, back-energy transfer).

measured in DMSO-d_6 on JEOL-ECX 500 FT (400 MHz) with TMS as a reference at 298 K. Solid-state FT-IR spectra were recorded from PerkinElmer model 1320 range of 400–4000 cm^{-1} using KBr discs. ESI-MS measurements of all the complexes [Ln(RnTPY)(TTA)$_3$](**1–9**) were carried out on WATERS Q-TOF Premier spectrometer. Electronic absorption spectra were recorded on a Varian V760 spectrophotometer, and the emission spectra were measured over an Agilent Carey Eclipse fluorescence spectrophotometer. All the analogous terpyridine derivatives (RnTPY) were synthesized by the known literature procedure mediated by Claisen–Schmidt condensation reaction, and these are all well-characterized by literature-reported data [46].

4.2. Synthesis and characterization

Synthesis of terpyridine derivatives (RnTPY): All the substituted terpyridine derivatives (viz. RnTPY, where n = 2, 3, 4) were synthesized by a published procedure mediated by the Claisen-Schmidt reaction. All the derivatives were thoroughly characterized and matches with reported data [46,70,71].

Synthesis of complexes [Ln(RnTPY)(TTA)$_3$] (1–9): All the complexes (**1–9**) were synthesized following our previously reported work [46,72].

[Eu(R2TPY)(TTA)$_3$] (1): Yield: 78%. FT-IR (KBr/ cm^{-1}) ν: 3432 (w, br, $\nu_{O—H}$), 1612 (s, $\nu_{C=O}$),1574 (m), 1536 (s), 1502 (m), 1471 (m), 1414 (s), 1355 (s), 1301 (s), 1243 (m), 1229 (s), 1184 (s), 1140 (s), 1059 (m), 1031 (w), 1010 (m), 933 (m), 885 (m), 859 (m), 780 (s, ν_{CF3}), 746 (m), 717 (m), 693 (m), 679 (m), 660 (m), 652 (m), 642 (m), 605 (m), 578 (s), 519 (w, ν_{Eu-N}), 498 (w, ν_{Eu-O}). Elemental analysis: Calcd. for $C_{44}H_{26}EuF_9N_4O_6S_3$, C, 46.94; H, 2.33; N, 4.98. Found: C, 46.78; H, 2.47; N, 4.84. ESI-MS (*m/z*): [M-TTA]$^+$ calcd for $C_{36}H_{22}N_4O_4F_6S_2Eu$, 905.0199; found, 905.0115. UV–vis [DMF, λ/nm (ε/M^{-1} cm^{-1})]: 336 (52,842), 280 (50,742).

[Eu(R3TPY)(TTA)$_3$] (2): Yield: 72%. FT-IR (KBr/ cm^{-1}) ν: 3406 (w, br, $\nu_{O—H}$), 1607 (s, $\nu_{C=O}$),1576 (m), 1538 (s), 1499 (m), 1470 (m), 1414 (s), 1357 (s), 1307 (s), 1242 (m), 1228 (s), 1177 (s), 1139 (s), 1057 (m), 1029 (w), 1011 (m), 934 (m), 890 (m), 858 (m), 783 (s, ν_{CF3}), 748 (m), 712 (m), 693 (m), 680 (m), 654 (m), 640 (m), 604 (m), 579 (s), 519 (w, ν_{Eu-N}), 500 (w, ν_{Eu-O}). Elemental analysis: Calcd. for $C_{44}H_{26}EuF_9N_4O_6S_3$, C, 46.94; H, 2.33; N,4.98. Found: C, 46.85; H, 2.51; N, 4.82. ESI-MS (*m/z*): [M-TTA]$^+$ calcd for$C_{36}H_{22}N_4O_4F_6S_2Eu$, 905.0199; found, 905.0204. UV–vis [DMF, λ/nm (ε/M^{-1} cm^{-1})]: 336 (57,370), 280 (46,797).

[Eu(R4TPY)(TTA)$_3$] (3): Yield: 74%. FT-IR (KBr/ cm^{-1}) ν: 3424 (w, br, $\nu_{O—H}$), 1612 (s, $\nu_{C=O}$), 1575 (m), 1536 (s), 1502 (m), 1475 (m), 1414 (s), 1355 (s), 1302 (s), 1243 (m), 1230 (s), 1184 (s), 1140 (s), 1060 (m), 1031 (w), 1011 (m), 934 (m), 882 (m), 859 (m), 784 (s, ν_{CF3}), 767 (m), 715 (m), 693 (m), 679 (m), 653 (m), 639 (m), 604 (m), 579 (s), 458 (w). Elemental analysis: Calcd. for $C_{44}H_{26}EuF_9N_4O_6S_3$, C, 46.94; H, 2.33; N, 4.98. Found: C, 46.91; H, 2.42; N, 4.94. ESI-MS (*m/z*): [M-TTA]$^+$ calcd for $C_{36}H_{22}N_4O_4F_6S_2Eu$, 905.0199; found, 905.0040. UV–vis: [DMF, λ/nm (ε/M^{-1} cm^{-1})] 336 (38,704), 280 (34,365).

[Sm(R2TPY)(TTA)$_3$] (4): Yield: 76%. FT-IR (KBr/ cm^{-1}) ν: 3441 (w, br, $\nu_{O—H}$), 1611 (s, $\nu_{C=O}$), 1575 (m), 1537 (s), 1502 (m), 1470 (m), 1414 (s), 1356 (s), 1304 (s), 1244 (m), 1230 (s), 1185 (s), 1140 (s), 1060 (m), 1033 (w), 1012 (m), 934 (m), 882 (m), 859 (m), 781 (s, ν_{CF3}), 718 (m), 693 (m), 680 (m), 660 (m), 653 (m), 642 (m), 605 (m). Elemental analysis: Calcd. for $C_{48}H_{32}F_9N_6O_6S_3Sm$, C, 47.79; H, 2.67; N, 6.97. Found: C, 47.65; H, 2.58; N, 6.89. ESI-MS (*m/z*): [M-TTA]$^+$ calcd for $C_{36}H_{22}N_4O_4F_6S_2Sm$, 904.0184; found, 904.0244. UV–vis: [DMF, λ/nm (ε/M^{-1} cm^{-1})] 336 (45,220), 280 (37,844).

[Sm(R3TPY)(TTA)$_3$] (5): Yield: 67%. FT-IR (KBr/ cm^{-1}) ν: 3423 (w, br, $\nu_{O—H}$), 1611 (s, $\nu_{C=O}$), 1537 (s), 1501 (m), 1471 (m), 1414 (s), 1356 (s), 1304 (s), 1244 (m), 1230 (s), 1185 (s), 1140 (s), 1060 (m), 1011 (m), 934 (m), 882 (m), 859 (m), 784 (s, ν_{CF3}), 717 (m), 679 (m), 654 (m), 641 (m), 580 (s), 436 (w). Elemental analysis: Calcd. for $C_{48}H_{32}F_9N_6O_6S_3Sm$, C, 47.79; H, 2.67; N, 6.97. Found: C, 47.68; H, 2.57; N, 6.93. ESI-MS (*m/z*): [M-TTA]$^+$ calcd for $C_{36}H_{22}N_4O_4F_6S_2Sm$, 904.0184; found, 904.0291. UV–vis [DMF, λ/nm (ε/M^{-1} cm^{-1})]: 336 (40,624), 282 (37,162).

[Sm(R4TPY)(TTA)$_3$] (6): Yield: 68%. FT-IR (KBr/ cm^{-1}) ν: 3431 (w, br, $\nu_{O—H}$), 1609 (s, $\nu_{C=O}$),1582 (m), 1538 (s), 1504 (m), 1470 (m), 1413 (s), 1356 (s), 1303 (s), 1245 (m), 1230 (s), 1186 (s), 1140 (s), 1060 (m), 1042 (w), 1011 (m), 933 (m), 881 (m), 859 (m), 790 (s, ν_{CF3}), 751 (m), 719 (m), 693 (m), 680 (m), 656 (m), 642 (m), 605 (m), 580 (s), 458 (w). Elemental analysis: Calcd. for $C_{44}H_{26}F_9N_4O_6S_3Sm$, C, 47.01; H, 2.33; N, 4.98. Found: C, 47.09; H, 2.25; N, 5.06. ESI-MS (*m/z*): [M-TTA]$^+$ calcd for $C_{36}H_{22}N_4O_4F_6S_2Sm$, 904.0184; found, 904.0158. UV–vis [DMF, λ/nm (ε/M^{-1} cm^{-1})]: 336 (38,704), 280 (34,365).

[Dy(R2TPY)(TTA)$_3$] (7): Yield: 68%. FT-IR (KBr/ cm^{-1}) ν: 3432 (w, br, $\nu_{O—H}$), 1614 (s, $\nu_{C=O}$), 1538 (s), 1502 (m), 1471 (m), 1413 (s),1393 (w), 1354 (s), 1307 (s), 1245 (m), 1231 (s), 1187 (s), 1140 (s), 1061 (m), 1014 (m), 935 (m), 882 (m), 859 (m), 780 (s, ν_{CF3}), 728 (m), 681 (m), 660 (m), 654 (m), 642 (m), 605 (m), 581 (s). Elemental analysis: Calcd. for $C_{48}H_{32}DyF_9N_6O_6S_3$, C, 47.32; H, 2.65; N, 6.90. Found: C, 47.43; H, 2.68; N, 6.81. ESI-MS (*m/z*): [M-TTA]$^+$ calcd for $C_{36}H_{22}N_4O_4F_6S_2Dy$, 916.0278; found, 916.0303. UV–vis [DMF, λ/nm (ε/M^{-1} cm^{-1})]: 336 (46,278), 280 (54,452).

[Dy(R3TPY)(TTA)$_3$] (8): Yield: 66%. FT-IR (KBr/ cm^{-1}) ν: 3431 (w, br, $\nu_{O—H}$), 1614 (s, $\nu_{C=O}$), 1538 (s), 1502 (m), 1467 (m), 1413 (s), 1357 (s), 1308 (s), 1246 (m), 1231(s), 1187 (s), 1140 (s), 1061 (m), 1032 (w), 1014 (m), 935 (m), 882 (m), 859 (m), 787 (s, ν_{CF3}), 768 (m), 716 (m), 694 (m), 681 (m), 661 (m), 643 (m), 606 (m), 581 (s), 459 (w), 419. Elemental analysis: Calcd. for $C_{45}H_{30}DyF_9N_4O_7S_3$, C, 46.26; H, 2.59; N, 4.80. Found: C, 47.21; H, 2.48; N, 4.88. ESI-MS (*m/z*): [M-TTA]$^+$calcd for $C_{36}H_{22}N_4O_4F_6S_2Dy$, 916.0278; found, 916.0201. UV–vis DMF, λ/nm (ε/M^{-1} cm^{-1})]: 336 (41, 600), 280 (48,880).

[Dy(R4TPY)(TTA)$_3$] (9): Yield: 73%. FT-IR (KBr/ cm-1) ν: 3442 (w, br, $\nu_{O—H}$), 1610(s, $\nu_{C=O}$),1582 (m), 1539 (s), 1513 (m), 1470 (m), 1413 (s), 1357 (s), 1307 (s), 1247 (m), 1231 (s), 1187 (s), 1140 (s), 1061 (m), 1041 (w), 999 (m), 935 (m), 859 (m), 791 (s, ν_{CF3}), 769 (m), 719 (m), 694 (m), 682 (m), 669 (m), 656 (m), 644 (m), 606 (m), 582 (s), 511 (w), 462(w), 415(w). Elemental analysis: Calcd. for $C_{45}H_{30}DyF_9N_4O_7S_3$, C: 46.26; H, 2.59; N, 4.80. Found: C, 47.18; H, 2.55; N, 4.92. ESI-MS (*m/z*): [M-TTA]$^+$ calcd for $C_{36}H_{22}N_4O_4F_6S_2Dy$, 916.0278; found, 916.0201. UV–vis [DMF, λ/nm (ε/M^{-1} cm^{-1})]: 336 (41,105), 280 (53,294).

4.3. Computational details

The molecular geometries for the investigated complexes were derived from crystallographic data, with computational optimization restricted solely to hydrogen atom positions this allows to keep the geometry imposed by crystal packing. In case of [Ln(RnTPY)(TTA)$_3$] (**8** and **9**) complexes (Ln = Dy^{III}, Rn = R3, R4) geometries were optimized using the [Dy(R2TPY)(TTA)$_3$] coordinates as reference. Geometry optimizations were performed by employing the BP86 generalized gradient approximation (GGA) functional along with the Slater–type orbital (STO) basis set TZP [73–75]. Scalar relativistic (SR) effects were included through a two-component Hamiltonian with the zeroth-order regular approximation (ZORA) [76]. The calculations were carried out in the ADF program. To ensure consistency across the three families, the optimized geometries were compared against experimental crystallographic data. No significant structural deviations were observed; specifically, the atomic positions within the first coordination sphere exhibited a Root-Mean-Square Deviation (RMSD) of <5%. These results validate the level of theory employed in the construction of both models.

To get more insight into the electronic structure and elucidate the most probable energy transfer pathways of each system, the fragmentation scheme proposed in a previous work was applied [62]. The idea is to treat both ligand and lanthanide fragments at the same level of theory, but separately. However, to evaluate any effect coming from the modification of the RnTPY ligand over the lanthanide center, no lanthanide-containing fragments were considered. It means that the lanthanide energy levels were obtained considering the entire complex. In this sense, two fragments were defined for each system, the [RnTPY]

(Rn = R2, R3, and R4) and the [TTA] ligands (Scheme 1). Then, the CASSCF/NEVPT2 methodology was applied to these fragments and on the entire complexes to recover part of the correlation energy and achieve an appropriate description of ground and excited states.

The use of this strategy requires, as the first step, a starting wave function that in this case corresponds to a KS–DFT (Kohn–Sham density functional theory) calculated at the PBE0 level of theory in conjunction with the def2–TZVP basis set for all the atoms except the lanthanides (Sm^{III}, Eu^{III}, Dy^{III}) which were treated with the SARC2–DKH–QZV basis set [77–79]. Scalar relativistic effects were incorporated *via* the second-order Douglas–Kroll–Hess (DKH2) Hamiltonian [80]. The resulting wave functions were employed to perform state–average (SA) CASSCF calculations. The complete active space self–consistent field (CASSCF) method recovers static and part of the dynamic correlation [81]. It divides the canonical orbital space (doubly occupied orbitals), virtual (empty orbitals), and active (fractionally occupied orbitals) subspaces; in the latter, a full–configuration interaction (CI) is performed. The idea is to obtain wave functions that can be thought as the corresponding Russell−Saunders terms, whose degeneracies are weakly split by the presence of the ligand environment. To accomplish this, a minimal active space was chosen for the $[M(RnTPY)(TTA)_3]$ systems and consisted of *n* electrons in seven 4*f* orbitals, CAS(n,7), n = 5, 6, 9 for Sm^{III}, Eu^{III}, Dy^{III} respectively. Then, an expansion was done by including the 5*d* shell, CAS (n, 12). In the case of the fragments (corresponding to the ligands) an active space of 8 electrons in 8 orbitals, CAS (8, 8), was employed. Scalar relativistic effects were included through the DKH2 Hamiltonian, while spin- orbit (SO) coupling through quasi–degenerate perturbation theory (QDPT) [82]. The remaining dynamical correlation was recovered by n–electron valence state perturbation theory (NEVPT2) that, unlike CASSCF, considers excitations (singles and doubles) between the subspaces previously defined. All these calculations were performed using the ORCA 4.2.1 package [83].

CRediT authorship contribution statement

Zafar Abbas: Writing – review & editing, Writing – original draft, Methodology, Investigation, Formal analysis, Conceptualization. **Usha Yadav:** Writing – review & editing, Writing – original draft, Methodology, Investigation, Formal analysis, Data curation, Conceptualization. **Ray J. Butcher:** Visualization, Validation, Investigation. **María Joaquina Beltrán-Leiva:** Writing – original draft, Methodology, Investigation, Formal analysis, Data curation. **Julián Santoyo-Flores:** Writing – original draft, Methodology, Investigation, Formal analysis. **Dayán Páez-Hernández:** Writing – review & editing, Validation, Supervision. **Ashis K. Patra:** Writing – review & editing, Validation, Supervision, Conceptualization.

Declaration of competing interest

All the authors Usha Yadav, Zafar Abbas, Ray J. Butcher, Julián Santoyo-Flores, Dayán Páez-Hernández, and Ashis K. Patra, declare that they have no known competing financial interests or personal relationships that could have appeared to influence the work reported in this paper.

Acknowledgements

We thank IIT Kanpur for infrastructure and the Science and Engineering Research Board (SERB) for financial support (EMR/2016/000521). Zafar Abbas and Usha Yadav thank the University Grants Commission (UGC) for research fellowships. The theoretical work has been supported by the Grants FONDECYT No 1150629 and 1180017. María Joaquina Beltrán-Leiva acknowledges CONICYT/Doctorado Nacional 2015/ 21151553 and Julián Santoyo-Flores acknowledges national Agency for Research and Development [ANID-PFCHA/Doctorado-Nacional/2019–21190164] for their PhD fellowships.

Supplementary materials

Supplementary material associated with this article can be found, in the online version, at doi:10.1016/j.molstruc.2026.147364.

Data availability

Data will be made available on request.

References

[1] J.C.G. Bünzli, C. Piguet, Chem. Soc. Rev. 34 (2005) 1048.
[2] Z. Zhang, Q. Han, J.W. Lau, B. Xing, ACS Mater. Lett. 2 (2020) 1516–1531.
[3] A. De Bettencourt-Dias, Dalton Trans. (2007) 2229–2241.
[4] Z.R. Hong, C.J. Liang, R.G. Li, W.L. Li, D. Zhao, D. Fan, D.Y. Wang, B. Chu, F. X. Zang, L.S. Hong, S.T. Lee, Adv. Mater. 13 (2001) 1241.
[5] J. Yu, L. Zhou, H. Zhang, Y. Zheng, H. Li, R. Deng, Z. Peng, Z. Li, Inorg. Chem. 44 (2005) 1611–1618.
[6] G. Bao, J. Lumin. 228 (2020) 117622.
[7] M.L. Aulsebrook, B. Graham, M.R. Grace, K.L. Tuck, Coord. Chem. Rev. 375 (2018) 191–220.
[8] M.C. Heffern, L.M. Matosziuk, T.J. Meade, Chem. Rev. 114 (2014) 4496–4539.
[9] S.V. Bünzli, J.-C.G. Eliseeva, Lanthanide Luminescence, 7, Springer, Berlin Heidelberg, Berlin, Heidelberg, 2011, pp. 1–275.
[10] L. Armelao, S. Quici, F. Barigelletti, G. Accorsi, G. Bottaro, M. Cavazzini, E. Tondello, Coord. Chem. Rev. 254 (2010) 487–505.
[11] G.de Sá, O. Malta, C.de Mello Donegá, A. Simas, R. Longo, P. Santa-Cruz, E.. da Silva, Coord. Chem. Rev. 196 (2000) 165–195.
[12] J.C.G. Bünzli, Acc. Chem. Res. 39 (2006) 53–61.
[13] E.G. Moore, A.P.S. Samuel, K.N. Raymond, Acc. Chem. Res. 42 (2009) 542–552.
[14] I. Hemmilä, V. Laitala, J. Fluoresc. 15 (2005) 529–542.
[15] P. Gawryszewska, J. Sokolnicki, J. Legendziewicz, Coord. Chem. Rev. 249 (2005) 2489–2509.
[16] C. Freund, W. Porzio, U. Giovanella, F. Vignali, M. Pasini, S. Destri, A. Mech, S. Di Pietro, L. Di Bari, P. Mineo, Inorg. Chem. 50 (2011) 5417–5429.
[17] P.A. Tanner, C.K. Duan, Coord. Chem. Rev. 254 (2010) 3026–3029.
[18] A.N. Kornblatt, P.H. Urband, A.C. Steere, J. Am, Vet. Med. Assoc. 186 (1985) 960–964.
[19] A. Bencini, V. Lippolis, Coord. Chem. Rev. 254 (2010) 2096–2180.
[20] C.R. De Silva, J. Li, Z. Zheng, L.R. Corrales, J. Phys. Chem. A 112 (2008) 4527–4530.
[21] A. Beeby, I.M. Clarkson, R.S. Dickins, S. Faulkner, D. Parker, L. Royle, A.S. De Sousa, J.A.G. Williams, M. Woods, J. Chem. Soc. Perkin Trans. 2 2 (1999) 493–504.
[22] W.H. William De, D.R. Sudnick, J. Am. Chem. Soc. 101 (1979) 334–340.
[23] A.P. Bassett, S.W. Magennis, P.B. Glover, D.J. Lewis, N. Spencer, S. Parsons, R. M. Williams, L. De Cola, Z. Pikramenou, J. Am. Chem. Soc. 126 (2004) 9413–9424.
[24] M.L.P. Reddy, V. Divya, R. Pavithran, Dalt. Trans. 42 (2013) 15249.
[25] S.I. Weissman, J. Chem. Phys. 10 (1942) 214–217.
[26] Z. Abbas, S. Dasari, M.J. Beltrán-Leiva, P. Cantero-López, D. Páez-Hernández, R. Arratia-Pérez, R.J. Butcher, A.K. Patra, New J. Chem. 43 (2019) 15139–15152.
[27] K. Gupta, A.K. Patra, Eur. J. Inorg. Chem. 2018 (2018) 1882–1890.
[28] S. Dasari, S. Singh, S. Sivakumar, A.K. Patra, Chem. - A Eur. J. 22 (2016) 17387–17396.
[29] M.L.P. Reddy, V. Divya, R. Pavithran, Dalton Trans. 42 (2013) 15249.
[30] U. Yadav, Z. Abbas, R.J. Butcher, A.K. Patra, New. J. Chem. 46 (2022) 18285–18294.
[31] U. Yadav, Z. Abbas, R.J. Butcher, A.K. Patra, Sensors Actuators B Chem. 375 (2023) 132938.
[32] A.J. Amoroso, S.J.A. Pope, Chem. Soc. Rev. 44 (2015) 4723–4742.
[33] K.X. Yu, J.G.C. Kragskow, Y.S. Ding, Y.Q. Zhai, D. Reta, N.F. Chilton, Y.Z. Zheng, Chem. 6 (2020) 1777–1793.
[34] R. Marin, G. Brunet, M. Murugesu, Angew. Chemie - Int. Ed. 60 (2021) 1728–1746.
[35] P. Jia, Z. Wang, Y. Zhang, D. Zhang, W. Gao, Y. Su, Y. Li, C. Yang, Spectrochim. Acta - Part A Mol. Biomol. Spectrosc. 230 (2020) 118084.
[36] W.T. Carnall, P.R. Fields, K. Rajnak, J. Chem. Phys. 49 (1968) 4424–4442.
[37] R.T. Wegh, H. Donker, K.D. Oskam, A. Meijerink, Science (1979) 283 (1999) 663–666.
[38] I. Hemmilá, V.M. Mukkala, Crit. Rev. Clin. Lab. Sci. 38 (2001) 441–519.
[39] D. Parker, Coord. Chem. Rev. 205 (2000) 109–130.
[40] P.A. Tanner, L. Zhou, C. Duan, K.L. Wong, Chem. Soc. Rev. 47 (2018) 5234–5265.
[41] O.L. Malta, J. Non Cryst. Solids 354 (2008) 4770–4776.
[42] F.R. Gonçalves e Silva, O.L. Malta, C. Reinhard, H.-U. Güdel, C. Piguet, J.E. Moser, J.-C.G. Bünzli, J. Phys. Chem. A 106 (2002) 1670–1677.
[43] P.P. Lima, S.S. Nobre, R.O. Freire, S.A. Júnior, R.A. Sá Ferreira, U. Pischel, O. L. Malta, L.D. Carlos, J. Phys. Chem. C 111 (2007) 17627–17634.
[44] M.J. Beltrán-Leiva, P. Cantero-López, C. Zúñiga, A. Bulhões-Figueira, D. Páez-Hernández, R. Arratia-Pérez, Inorg. Chem. 56 (2017) 9200–9208.
[45] M.J. Beltrán-Leiva, D. Páez-Hernández, R. Arratia-Pérez, Inorg. Chem. 57 (2018) 5120–5132.
[46] Z. Abbas, S. Dasari, M.J. Beltrán-Leiva, P. Cantero-López, D. Páez-Hernández, R. Arratia-Pérez, R.J. Butcher, A.K. Patra, New J. Chem. 43 (2019) 15139–15152.
[47] D.B. Ambili Raj, S. Biju, M.L.P. Reddy, Inorg. Chem. 47 (18) (2008) 8091–8100.

[48] M. Melegari, V. Marzaroli, R. Polisicchio, D. Seletti, L. Marchiò, V.L. Pecoraro, M. Tegoni, Inorg. Chem. 62 (27) (2023) 10645–10654.
[49] T.V. Quoc, L.N. Ngoc, V. Do Truc, L.D. Khanh, H.H. Manh, C.T. Pham, L. Van Meervelt, Acta Crystallogr. Sect. E Crystallogr. Commun. 73 (2017) 1389–1392.
[50] G.J. Visser, G.J. Heeres, J. Wolters, A. Vos, Acta Crystallogr. Sect. B Struct. Crystallogr. Cryst. Chem. 24 (1968) 467–473.
[51] U. Yadav, M. Verma, Z. Abbas, S. Sivakumar, A.K. Patra, New. J. Chem. 46 (2022) 16007–16018.
[52] R.M. Supkowski, W.D.W. Horrocks, Inorganica Chim. Acta 340 (2002) 44–48.
[53] L.J. Daumann, D.S. Tatum, B.E.R. Snyder, C. Ni, G.-l. Law, E.I. Solomon, K. N. Raymond, J. Am. Chem. Soc. 137 (2015) 2816–2819.
[54] M. Cui, A.-L. Wang, C.-L. Gao, L. Zhou, T. Wu, S. Fang, H.-P. Xiao, F.-C. Li, X.-L. Li, Dalton Trans. 50 (2021) 1007–1018.
[55] H. Wang, H. Li, Y. Zhang, X. Chen, J. Mol. Struct. 1270 (2022) 133956, 1270.
[56] J.C.G. Bünzli, Handb. Phys. Chem. Rare Earths 50 (2016) 141–176.
[57] M.J. Beltrán-Leiva, D. Páez-Hernández, R. Arratia-Pérez, Inorg. Chem. 57 (2018) 5120–5132.
[58] J.G. Bünzli, Coord. Chem. Rev. (2015) 19–47, 293–294.
[59] T.D. Brown, T.M. Shepherd, J. Chem. Soc., Dalton Trans. (1973) 336.
[60] M. Shi, F. Li, T. Yi, D. Zhang, H. Hu, C. Huan, Inorg. Chem. 44 (2005) 8929–8936.
[61] A.P.S. Samuel, J. Xu, K.N. Raymond, Inorg. Chem. 48 (2009) 687–698.
[62] M.J. Beltrán-Leiva, P. Cantero-López, C. Zúñiga, A. Bulhões-Figueira, D. Páez-Hernández, R. Arratia-Pérez, Inorg. Chem. 56 (2017) 9200–9208.
[63] C.G. Ma, M.G. Brik, D.X. Liu, B. Feng, Y. Tian, A. Suchocki, J. Lumin. 170 (2016) 369–374.
[64] A.N.C. Neto, R.T. Moura Jr, L.D. Carlos, O.L. Malta, M. Sanadar, A. Melchior, E. Kraka, S. Ruggieri, M. Bettinelli, F. Piccinelli, Inorg. Chem. 61 (41) (2022) 16333–16346.
[65] M. Latva, H. Takalo, V.-M. Mukkala, C. Matachescu, J.C. Rodriguez-Ubis, J. Kankarea, J. Lumin. 75 (1997) 149–169.
[66] D. Parker, J.D. Fradgley, M. Delbianco, M. Starck, J.W. Walton, J.M. Zwier, Faraday Discuss. 234 (2022) 159–174.
[67] R.A.S. Ferreira, E. Mamontova, A.M.P. Botas, M. Shestakov, Johan Vanacken, V. Moshchalkov, Y. Guari, L.F. Chibotaru, D. Luneau, P.S. André, J. Larionova, J. Long, L.D. Carlos, Adv. Optical Mater. 9 (2021) 2101495.
[68] J. Corredoira-Vázquez, C. González-Barreira, A.M. García-Deibe, J. Sanmartín-Matalobos, M.A. Hernández-Rodríguez, C.D.S. Brites, L.D. Carlos, M. Fondo, Inorg. Chem. Front. 11 (2024) 1087–1098.
[69] Y. Gil, R. Gimeno-Muñoz, R. Costa de Santana, N. Aliaga-Alcalde, P. Fuentealba, D. Aravena, A. González-Campo, E. Spodine, Inorg. Chem. 61 (2022) 16347–16355.
[70] A. Maroń, A. Szlapa, T. Klemens, S. Kula, B. Machura, S. Krompiec, J.G. Małecki, A. Świtlicka-Olszewska, K. Erfurt, A. Chrobok, Org. Biomol. Chem. 14 (2016) 3793–3808.
[71] J. Husson, L. Guyard, Heterocycl. Commun. 21 (2015) 199–202.
[72] Zafar Abbas, Usha Yadav, Ray J. Butcher, Ashis K. Patra, J. Mater. Chem. C 9 (2021) 10037–10051.
[73] J.P. Perdew, W. Yue, Phys. Rev. B 33 (1986) 8800–8802.
[74] J.P. Perdew, K. Burke, M. Ernzerhof, Phys. Rev. Lett. 77 (1996) 3865–3868.
[75] E. Van Lenthe, E.J. Baerends, J. Comput. Chem. 24 (2003) 1142–1156.
[76] F. Wang, T. Ziegler, J. Chem. Phys. 123 (2005) 15402–15412.
[77] C. Adamo, V. Barone, J. Chem. Phys. 110 (1999) 6158–6170.
[78] F. Weigend, R. Ahlrichs, Phys. Chem. Chem. Phys. 7 (2005) 3297.
[79] D.A. Pantazis, F. Neese, Theor. Chem. Acc. 131 (2012) 1–7.
[80] B.A. Hess, Phys. Rev. A 33 (1986) 3742–3748.
[81] P.O. Nelson, P. Thayumanavan, M.F. Azizian, K.J. Williamson, Water Pollut. 48 (2005) 271–291.
[82] C. Angeli, R. Cimiraglia, J.P. Malrieu, J. Chem. Phys. 117 (2002) 9138–9153.
[83] F. Neese, WileyInterdiscip, Rev. Comput. Mol. Sci. 12 (2022) 1–15.